Inorg. Chem. **2004**, *43*, 6805–6814

Functional Superoxide Dismutase Mimics. Structural Characterization and Magnetic Exchange Interactions of Copper(II)–N-Substituted Sulfonamide Dimer Complexes†

R. Cejudo-Marín, G. Alzuet, S. Ferrer, and J. Borrás*

Departamento de Química Inorgánica, Facultad de Farmacia, Universidad de Valencia, Avda. Vicent Andrés Estellés s/n, 46100-Burjassot, Spain

A. Castiñeiras

Departamento de Química Inorgánica, Facultad de Farmacia, Universidad de Santiago de Compostela, 15703-Santiago de Compostela, Spain

E. Monzani and L. Casella

Dipartimento di Chimica Generale, Università di Pavia, Via Taramelli 12, 27100-Pavia, Italy

Received March 4, 2004

Dinuclear copper(II) complexes with N-substituted sulfonamide ligands as superoxide dismutase (SOD) mimics have been investigated. The new *N*-(thiazol-2-yl)toluenesulfonamide (Htz-tol) and *N*-(thiazol-2-yl)naphthalenesulfonamide (Htz-naf) ligands have been prepared and structurally characterized. The complexes derived from these ligands, $[Cu_2(tz\text{-}tol)_4]$ (**1**) and $[Cu_2(tz\text{-}naf)_4]$ (**2**), have been synthesized, and their crystal structure, magnetic properties, and EPR spectra were studied in detail. In both compounds the metal centers are bridged by four nonlinear triatomic NCN groups. The coordination geometry of the coppers in the dinuclear entity of **1** and **2** is distorted square planar with two *N*-thiazole and two *N*-sulfonamido atoms. Magnetic susceptibility data show a strong antiferromagnetic coupling, with $-2J = 121.3$ cm^{-1} for compound **1** and $-2J = 104.3$ cm^{-1} for compound **2**. The EPR spectra of the polycrystalline samples of compounds **1** and **2** have been measured at the X- and Q-band frequencies at different temperatures. Above 20 K the spectra are characteristic of $S = 1$ species with zero-field splitting parameter $D = 0.230$ cm^{-1} for compound **1** and 0.229 cm^{-1} for compound **2**. The EPR parameters are discussed in terms of the known binuclear structures. The complexes exhibit high SOD activity, as shown by the low IC_{50} values obtained with the xanthine/xanthine oxidase/NBT assay: 0.13 μM for compound **1**; 0.17 μM for compound **2**.

Introduction

Superoxide anion radical is a metabolite of oxygen in vivo and is considered to be a highly toxic species in many living systems.[1] It is involved in lipid peroxidation, DNA damage, aging, cancer, and many other diseases. Superoxide dismutase (SOD) is an efficient scavenger of $O_2^{\bullet -}$ and plays an important role in the protection of cells against its toxicity effects. However, in the case of an oxygen burst, these enzymes are insufficient in vivo. The clinical efficacy of SOD has been disappointing because SOD enzymes have molecular weights too high to cross the cell membranes. Studies on the reactivity of low molecular weight copper complexes which have a SOD-like function have attracted much attention for the development of SOD mimics and for expanding the biomimetic chemistry of transition metal complexes. For many years efforts have been made to obtain compounds with high catalytic activity. Among the most successful compounds possessing SOD activity are dinuclear

* Author to whom correspondence should be addressed. E-mail: joaquin.borras@uv.es. Tel: ++34 963544530. Fax: ++34 963544960.

† Abbreviations: Htz-naf = *N*-(thiazol-2-yl)naphthalenesulfonamide; Htz-tol = *N*-(thiazol-2-yl)toluenesulfonamide; MF^+ = blue formazane; NBT = nitro blue tetrazolium; SOD = superoxide dismutase.

(1) Sawyer, D. T.; Valentine, J. S. *Acc. Chem. Res.* **1981**, *14*, 393.

10.1021/ic049718w CCC: $27.50
Published on Web 09/15/2004

copper complexes.[2−4] Important requirements for SOD-like activity appear to be a medium strength donor power and the flexibility of the ligands. Interestingly, the presence of coordination sites belonging to N heteroaromatic rings is considered an important factor for gaining high SOD activity.

We have previously reported a variety of mononuclear Cu(II) compounds with sulfathiazole (4-amino-*N*-(thiazol-2-yl)-benzenesulfonamide) and imidazole, imidazole derivatives or pyridine that exhibit high SOD-like activity.[5−7] Also, we have prepared and fully characterized a dinuclear copper compound of sulfathiazolato.[8] In this compound, classified as a type IV copper dimer,[9] the two metal ions are bridged by four nonlinear triatomic NCN groups. These triatomic units are found in biological molecules such as adenine.[10,11] More recently, we have described the crystal structure and properties of a dicopper(II) complex with sulfamethazine (4-amino-*N*-[4,6-dimethyl-2-pyrimidinyl]benzenesulfonamide) bridged by two carboxylato anions and by two NCN fragments of the ligand.[12] Both compounds display interesting magnetic and EPR behavior. DFT studies have shown the nature of the antiferromagnetic interaction between the two copper(II) at a very short distance.

As an extension of our studies of sulfonamide derivatives and their metal complexes, we have developed a new class of *N*-substituted sulfonamide ligands based on thiazole units. This type of ligands possess important features for obtaining copper(II) complexes with high SOD-like activity: (i) nonlinear NCN fragments and, thus, the possibility of forming dinuclear compounds with relatively short Cu−Cu distances; (ii) a coordination site with nitrogen heteroaromatic donors; (iii) the ability of accommodating the copper ion in different geometries.

In this paper, we report the synthesis, crystal structures, magnetic properties, and SOD-like activity of two new dinuclear compounds possessing the above characteristics, $[Cu_2[tz\text{-}tol)_4]$ (Htz-tol = *N*-(thiazol-2-yl)toluenesulfonamide) and $[Cu_2[tz\text{-}naf)_4]$ (Htz-naf = *N*-(thiazol-2-yl)naftalenesulfonamide) (see Chart 1).

Chart 1

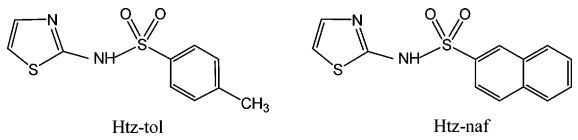

Experimental Section

Materials and Physical Methods. All reagents and chemicals were purchased from commercial sources and used without further purification. Elemental Analyses (C, H, N, S) were carried out at the microanalytical laboratory of the Instituto Tecnológico de Química (Universidad Politécnica de Valencia, Valencia, Spain). The infrared spectra (ν = 400−4000 cm^{-1}) were obtained on KBr pellets using a Mattson Satellite FTIR spectrophotometer. Electronic spectra were recorded on samples dispersed in Nujol mulls (solid) and on acetonitrile and acetone solutions using a Shimadzu 2101 PC spectrophotometer. The kinetic measurements were performed on a HP 8452A spectrophotometer. Electrochemical measurements were made using a Princeton Applied Research model 273A potentiostat/galvanostat. Cyclic voltammograms were obtained for acetone solutions of the complexes containing tetrabutylammonium perchlorate as the supporting electrolyte under argon atmosphere. The electrochemical cell employed was of a standard three-electrode configuration: platinum working electrode; platinum wire counter electrode; Ag−AgCl reference electrode. All the potentials were transformed to NHE scale. EPR measurements on ground crystals were carried out at variable temperature on a Bruker ELEXSYS spectrometer, operating at X-band and Q-band frequencies. Frozen-solution EPR spectra of the complexes were recorded in acetonitrile and acetone at 100 K. The variable-temperature magnetic susceptibility measurements on microcrystalline samples were taken with a Quantum Design MPMS2 SQUID susceptometer equipped with a 55 kG magnet, operating at 10 kG in the range of 1.8−400 K. The susceptometer was calibrated with $(NH_4)_2Mn(SO_4)_2{\cdot}12H_2O$. Corrections for the diamagnetism were estimated from the Pascal constants.

Synthesis of the Ligands: *N*-(Thiazol-2-yl)toluenesulfonamide (Htz-tol) and *N*-(Thiazol-2-yl)naphthalenesulfonamide (Htz-naf). A solution containing 2.0 g of 2-aminothiazole and 4.55 g of the corresponding sulfonyl chloride (*p*-toluenesulfonyl chloride or naphthalenesulfonyl chloride) in 12 mL of pyridine was heated to 60 °C for 1 h. The mixture was poured into 20 mL cold water and then stirred for several min. The resulting product was recrystallized from ethanol. Crystals suitable for X-ray diffraction were formed after 6 months. Yield: 72%, based on $C_{10}H_{10}N_2S_2O_2$ (Htz-tol) (M_r = 254.34). Anal. Calcd: C, 47.24; H, 3.94; N, 11.02; S, 25.20. Found: C, 47.81; H, 3.95; N, 10.81; S, 24.78. IR (KBr) (ν_{max}/cm^{-1}): 1541 (thiazole ring); 1329 and 1147 (SO_2); 934 (S−N). Yield: 65%, based on $C_{13}H_{10}N_2S_2O_2$ (Htz-naf) (M_r = 290.35). Anal. Calcd: C, 53.42; H, 3.42; N, 9.60; S, 21.92. Found: C, 53.84; H, 3.38; N, 9.41; S, 21.81. IR (KBr)(ν_{max}/cm^{-1}): 1540 (thiazole ring); 1306, 1279, 1141, and 1118 (SO_2); 928 (S−N).

Synthesis of the Complexes. (a) $[Cu_2[tz\text{-}tol)_4]$ (1). A 100 mL volume of an ethanolic solution containing 1 mmol of Htz-tol (0.254 g) was added to 50 mL of an ethanolic solution containing 0.5 mmol of $Cu(CF_3COO)_2$ (0.15 g). The resulting yellow mixture was left to stand at room temperature. After 7−8 days well-shaped dark red crystals suitable for X-ray diffraction were formed. Yield: 51%, based on $Cu_2C_{40}H_{36}N_8S_8O_8$ (M_r = 1140.33). Anal. Calcd: C, 42.13; H, 3.18; N, 9.83; S, 22.49. Found: C, 41.89; H, 2.93; N, 9.73; S, 22.82. IR (KBr) (ν_{max}/cm^{-1}): 1471 (thiazole ring); 1322, 1140 (SO_2); 948 (S−N). Solid-state electronic spectra (λ_{max}, nm): 510 (LF). UV−vis: in CH_3CN, λ_{max} = 490 nm (ϵ = 1070 mol^{-1} dm^3 cm^{-1}); in acetone, λ_{max} = 495 nm (ϵ = 992 mol^{-1} dm^3 cm^{-1}).

(b) $[Cu_2(tz\text{-}naf)_4]$ (2). The $[Cu_2(tz\text{-}naf)_4]$ compound was obtained by following the procedure described above, but in this case the

(2) Tabbi, G.; Driessen, V. L.; Reedikj, J.; Bonomo, R. P.; Veldman, N.; Spek, A. L. *Inorg. Chem.* **1997**, *36*, 1168.
(3) Zhang, J.-J.; Luo, Q.-H.; Long, De-L.; Chen, J.-T.; Li, F.-M.; Liu, A.-D. J. *Chem. Soc., Dalton Trans.* **2000**, 1893.
(4) Feng, C.-J.; Luo, K.-H.; Wang, Z.-L.; Shen, M.-C.; Wang, H.-W.; Zhao M.-H. *J. Inorg. Biochem.* **1999**, *75*, 1.
(5) Casanova, J.; Alzuet, G.; Borrás, J.; Latorre, J.; Sanaú, M.; García-Granda, S. J. *Inorg. Biochem.* **1995**, *60*, 219.
(6) Casanova, J.; Alzuet, G.; Borrás, J.; Carugo, O. *J. Chem. Soc., Dalton Trans.* **1996**, 2239.
(7) Casanova, J.; Alzuet, G.; Ferrer, S.; Latorre, J.; Ramirez, J. A.; Borrás, J. *Inorg. Chim. Acta* **2000**, *304*, 170.
(8) Casanova, J.; Alzuet, G.; Latorre, J.; Borrás, J. *Inorg. Chem.* **1997**, *36*, 2052.
(9) Hathaway, B. J. Copper. In *Comprehensive Coordination Chemistry*; Wilkinson G., Gillard R. D., Cleverty, J. A., Eds.; Pergamon Press: New York, 1987; Vol. 5.
(10) de Meester, P.; Goodgame, D. M. L.; Price, K. A.; Skapski, A. C. *Nature* **1971**, *229*, 191.
(11) de Meester, P.; Skapsk, A. C. *J. Chem. Soc A* **1971**, 2167.
(12) Gutierrez, L.; Alzuet, G.; Borrás, J.; Castiñeiras, A.; Rodriguez-Fortea, A.; Ruiz, E. *Inorg. Chem.* **2001**, *40*, 3089.

Htz-naf ligand was dissolved in 100 mL of acetone. Yield: 25%, based on $Cu_2C_{52}H_{36}N_8S_8O_8$ (M_r = 1284.45). Anal. Calcd: C, 48.68; H, 2.82; N, 8.72; S, 19.97. Found: C, 48.93; H, 2.73; N, 8.63; S, 19.82. IR (KBr) (ν_{max}/cm^{-1}): 1467 (thiazole ring); 1322, 1298, 1144, 1123 (SO_2); 954 (S−N). Solid-state electronic spectra (λ_{max}, nm): 500 (LF). UV−vis: in CH_3CN, λ_{max} = 500 nm (ϵ = 882 mol^{-1} dm^3 cm^{-1}); in acetone, λ_{max} = 498 nm (ϵ = 1272 mol^{-1} dm^3 cm^{-1}).

X-ray Structure Determination. (a) *N*-(Thiazol-2-yl)toluenesulfonamide (Htz-tol). Diffraction data were collected on an area detector equipped Kappa CCD single-crystal diffractometer, using a combination of φ and ω scans.[13] Data were integrated, scaled, and averaged by the HKL2000 package.[14] Crystal structures were solved by Patterson methods, using the program DIRDIF.[15] An empirical absorption correction was applied using XABS2.[16] Anisotropic least-squares refinement was carried out with SHELXL-97.[17] Atomic scattering factors were taken from ref 18. Plots were made with the ORTEP package.[19] All calculations were made at the Scientific Computer Center of the University of Oviedo and on the X-ray group computers.

(b) *N*-(Thiazol-2-yl)naphthalenesulfonamide (Htz-naf). An orange prismatic crystal of $C_{13}H_{10}N_2O_2S_2$ was mounted on a glass fiber and used for data collection. Cell constants and an orientation matrix for data collection were obtained by least-squares refinement of the diffraction data from 25 reflections in the range of 12.66 < θ < 37.42° on an Enraf Nonius MACH3 automatic diffractometer.[20] Data were collected at 293 K using Cu Kα radiation (λ = 1.541 84 Å) and the $\omega/2\theta$-scan technique and corrected for Lorentz and polarization effects.[21] A semiempirical absorption correction (ω-scans) was made.[22] The structure was solved by direct methods,[23] which revealed the position of all non-hydrogen atoms, and refined on F^2 by a full-matrix least-squares procedure using anisotropic displacement parameters.[17] All hydrogen atoms were located from difference Fourier maps and included as fixed contributions riding on attached C atoms with isotropic thermal parameters 1.3 times those of the respective C atoms. Atomic scattering factors were taken from ref 18. Molecular graphics were made with PLATON[24] and SCHAKAL.[25]

(c) [Cu$_2$(tz-tol)$_4$]. A red plate crystal of $[Cu(C_{10}H_9N_2O_2S_2)_2]_2$ was mounted on a glass fiber and used for data collection. Crystal data were collected using a Bruker SMART CCD 1000 diffractometer. The data were processed with SAINT[26] and corrected for absorption using SADABS (transmission factors: 0.925−0.797).[27] The structure was solved by direct methods and refined by full-matrix least-squares techniques against F^2 using the program SHELXS-97.[17] Positional and anisotropic atomic displacement parameters were refined for all non-hydrogen atoms. Hydrogen atoms were placed geometrically, and positional parameters were refined using a riding model. Isotropic atomic displacement parameters for hydrogen atoms were constrained to be 1.2 (1.5 for methyl groups). Atomic scattering factors were taken from ref 18. Molecular graphics were made with PLATON99.[24]

(d) [Cu$_2$(tz-naf)$_4$]. A red-brown block crystal of $[Cu(C_{26}H_{18}N_4O_4S_4)_2]_2$ was mounted on a glass fiber and used for data collection. Cell constants and an orientation matrix for data collection were obtained by least-squares refinement of the diffraction data from 25 reflections in the range of 11.210° < θ < 30.406° on an Enraf-Nonius CAD4 automatic diffractometer.[20] Data were collected using the ω-scan technique and corrected for Lorentz and polarization effects.[21] A semiempirical absorption correction (ω-scan) was made.[22] The structure was solved by Patterson and Fourier methods,[23] which revealed the position of all non-hydrogen atoms, and refined on F^2 by a full-matrix least-squares procedure using anisotropic displacement parameters.[17] Hydrogen atoms were introduced in the calculation in idealized positions [d(C−H) = 0.92 Å], and their atomic coordinates were recalculated after each cycle. They were given isotropic thermal parameters 20% higher than those of the carbon to which they are attached. Criteria of a satisfactory complete analysis were the value of the ratios of rms shift to standard deviation less than 0.001 and no significant features in final difference maps. Atomic scattering factors were taken from ref 18. Molecular graphics were from PLATON[24] and SCHAKAL.[25]

A summary of the crystal data, experimental details, and refinement results for Htz-tol, Htz-naf, complex **1**, and complex **2** are listed in Table 1.

SOD Assay. The SOD activity of the copper compounds was studied according to a modification of the xanthine/xanthine oxidase assay,[28] with NBT as a superoxide anion detecting agent.[29] The assay was carried out in 50 mM phosphate buffer, pH 7.8, in thermostated optical cells at 25.0 ± 0.1 °C. The kinetics of reduction of nitro blue tetrazolium (NBT) to blue formazane (MF^+) was monitored through the absorbance changes with time at 560 nm. In a typical experiment, solutions of NBT (0.23 mM) and xanthine (0.28 mM) were mixed in the cuvette and the reaction was started by addition of a concentrated xanthine oxidase solution (final volume 1600 μL). The xanthine oxidase concentration must be optimized to find the appropriate amount that causes a linear absorbance variation with time during the reading period (usually 60 s). Under these conditions the turnover concentration of superoxide remains constant during the assay. We found that with the optimized xanthine oxidase concentration a straight line is observed when ΔA_{560}/min is lower than 0.03. With larger initial rates the absorbance variation with time follows a parabolic behavior. The effect of the Cu complexes on the NBT reduction rates was evaluated by adding small amounts of a concentrated solution of each complex to the assay solution so that its final concentration in the cuvette varied from 0.05 to 10 μM. The

(13) *Nonius, BV, Collect*; Enraf-Nonius: Delft, The Netherlands, 1997−2000.
(14) Otwinowski, Z.; Minor, W. *Methods Enzymol.* **1997**, *276*, 307.
(15) Beurskens, P. T.; Beurskens, G.; de Gelder, R.; García-Granda, S.; Gould, R. O.; Israel, R.; Smits, J. M. M. *The DIRDIF-99 program system*; Technical Report of the Crystallography Laboratory; University of Nijmegen: Nijmegen, The Netherlands, 1999.
(16) Parkin, S.; Moezzi, B.; Hope, H. *J. Appl. Crystallogr.* **1995**, *28*, 53.
(17) Sheldrick, G. M. *SHELXL-97. Program for the Refinement of Crystal Structures*; University of Göttingen: Göttingen, Germany, 1997.
(18) *International Tables for Crystallography*; Kynoch Press: Birmingham, U.K., 1992 (present distributor Kluwer Academic Publishers, Dordrecht, The Netherlands); Vol. C, Tables 4.2.6.8 and 6.1.1.4.
(19) Farrugia, L. J. *J. Appl. Crystallogr.* **1997**, *30*, 565.
(20) *Nonius, BV CAD4-Express Software*, ver. 5.1/1.2; Enraf-Nonius: Delft, The Netherlands, 1994.
(21) Kretschmar, M. *GENHKL Program for the Reducction of CAD4 Diffractometer Data*; University of Tuebingen: Tuebingen, Germany, 1997.
(22) North, A. C. T.; Phillips, D. C.; Mathews, F. S. *Acta Crystallogr.* **1968**, *A24*, 351.
(23) Sheldrick, G. M. *Acta Crystallogr.* **1990**, *A46*, 467.
(24) Spek, A. L. *PLATON. A Multipurpose Crystallographic Tool*; Utrecht University: Utrecht, The Netherlands, 2000.
(25) Keller, E. *SCHAKAL-97. A computer program for the graphic representation of molecular and crystallographyc models*; University of Freiburg i. Br.: Freiburg, Germany, 1997.
(26) *Bruker SMART and SAINT, Area Detector Control and Integration Software*; Bruker Analytical X-ray Instruments Inc.: Madison, WI, 1997.
(27) Sheldrick, G. M. *SADABS, Program for Empirical Absorption Correction of Area Detector Data*; University of Goettingen: Goettingen, Germany, 1997.
(28) Beauchamp, C.; Fridovich I. *Anal. Biochem.* **1971**, *44*, 276.
(29) Bielski, B. H. J.; Shiue, G. G.; Bajuk, S. *J. Phys. Chem.* **1980**, *84*, 830.

Table 1. Crystal and Structure Refinement Data for Htz-tol, Htz-naf, $[Cu(tz\text{-}tol)_2]_2$ (**1**), and $[Cu(tz\text{-}naf)_2]_2$ (**2**)

param	Htz-tol	Htz-naf	$[Cu(tz\text{-}tol)_2]_2$ (**1**)	$[Cu(tz\text{-}naf)_2]_2$ (**2**)
empirical formula	$C_{10}H_{10}N_2O_2S_2$	$C_{13}H_{10}N_2O_2S_2$	$C_{40}H_{36}Cu_2N_8O_8S_8$	$C_{52}H_{36}Cu_2N_8O_8S_8$
fw	254.34	290.35	1140.33	1284.45
temp, K	293(2)	293(2)	291(2)	213(2)
wavelength, Å	1.5418	1.541 84	0.710 73	1.541 84
cryst system	monoclinic	monoclinic	monoclinic	triclinic
space group	$P2_1/a$	$P2_1/c$ (No. 14)	$C2/c$ (No. 15)	$P\bar{1}$ (No. 2)
unit cell dimens, Å and deg	$a = 13.21320(7)$	$a = 12.8179(15)$	$a = 27.174(3)$	$a = 12.8308(8)$, $\alpha = 66.679(15)$
	$b = 6.5384(3)$, $\beta = 110.135(2)$	$b = 9.1246(11)$, $\beta = 90.993(7)$	$b = 10.1931(10)$, $\beta = 122.025(2)$	$b = 14.964(2)$, $\beta = 82.525(11)$
	$c = 13.68250(5)$	$c = 11.0332(8)$	$c = 20.025(2)$	$c = 15.048(3)$, $\gamma = 83.314(9)$
V, Å^3	1109.83(5)	1290.2(2)	4702.6(8)	2624.0(7)
Z; calcd density, Mg/m^3	4; 1.522	4; 1.495	4; 1.611	2; 1.626
abs coeff, mm^{-1}	4.253	3.742	1.320	4.513
F(000)	528	600	2328	1308
cryst size, mm	$0.35 \times 0.32 \times 0.30$	$0.32 \times 0.20 \times 0.20$	$0.18 \times 0.16 \times 0.06$	$0.15 \times 0.10 \times 0.05$
θ range for data collcn, deg	6.77−69.69	3.45−72.89	1.77−28.06	5.34−65.03
limiting indices	$16 \le h \le 15$, $-7 \le k \le 6$, $-16 \le l \le 16$	$-15 \le h \le 15$, $0 \le k \le 11$, $0 \le l \le 13$	$-35 \le h \le 35$, $-13 \le k \le 12$, $-13 \le l \le 26$	$-1 \le h \le 15$, $-17 \le k \le 17$, $-17 \le l \le 17$
reflecn collcd/unique	3307/2058 [R(int) = 0.0292]	5452/2582 [R(int) = 0.0050]	15546/5654 [R(int) = 0.1197]	10245/8918 [R(int) = 0.0613]
completeness to θ deg; %	69.69; 98.8	72.89; 100.0	28.06; 98.9	65.03; 99.8
abs corr	empirical	Ψ-scans	SADABS	Ψ-scan
max and min transmn	0.3907 and 0.2881	0.5216 and 0.3806	0.9250 and 0.7971	0.8058 and 0.5509
refinement method	full-matrix least squares on F^2	full-matrix least squares on F^2	full-matrix least squares on F^2	full-matrix least squares on F^2
data/restraints/params	2058/0/169	2582/0/173	5654/0/298	8918/0/703
goodness-of-fit on F^2	2.096	1.086	0.711	1.020
final R indices [$I > 2\sigma(I)$]	R1 = 0.0463, wR2 = 0.1598	R1 = 0.0348, wR2 = 0.0971	R1 = 0.0505, wR2 = 0.0662	R1 = 0.0487, wR2 = 0.1042
R indices (all data)	R1 = 0.0518, wR2 = 0.1982	R1 = 0.0435, wR2 = 0.1039	R1 = 0.1960, wR2 = 0.0884	R1 = 0.1028, wR2 = 0.1224
largest diff peak and hole, e•Å^{-3}	0.371 and −0.625	0.271 and −0.300	0.338 and −0.418	0.527 and −0.525

Scheme 1

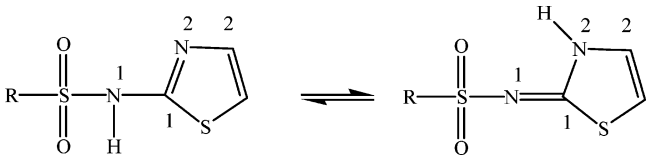

absorbance change at 560 nm with time upon addition of the xantine oxidase solution (as optimized in the previous step) was followed. Blank experiments were carried without xanthine oxidase to correct for the absorbance readings.

Results and Discussion

Crystal Structure of the Ligands. ORTEP drawings of the Htz-tol and Htz-naf ligands, bond distances (Å), and angles (deg) are deposited as Supporting Information. In general, angles and bond distances of the two ligands do not show significant features compared with related sulfonamides.[30,31] It is known that N-substituted sulfonamides exist as two tautomeric forms, amido and imido (see Scheme 1).

In the Htz-tol ligand the C(1)−N(1) bond distance [1.320(4) Å] is slightly shorter than the C(1)−N(2) one [1.342(4) Å], which seems to indicate that Htz-tol adopts mainly the imido form. However, for the Htz-naf ligand these bond lengths are found to be equal [C1−N1, 1.338(2) Å; C1−N2, 1.330(2) Å] suggesting an equilibrium between both amido and imido forms. In the two ligands, the dimensions of all the C−N distances do not support the existence of distinct C═N (average 1.316 Å) and C−N (average 1.416 Å) bonds due to an extensive π electron pair delocalization through the C(1)−N(1), C(1)−N(2), and C(2)−N(2) bonds. Atoms around the sulfonamide S atom are arranged in a distorted tetrahedral configuration with bond angles in the range from 104 to 119°. The C−C bond distances of the toluene ring in Htz-tol and those of the naphthalene ring in Htz-naf can be regarding as normal.

In the Htz-naf ligand the thiazole and naphthalene rings are nearly perpendicular to each other (angle between planes, 82.69°). The structure is stabilized by a strong hydrogen bond formed by the $N_{thiazole}$ and $N_{sulfonamido}$ (N−H···N distance, 2.849(2) Å).

Description of the Crystal Structures of $[Cu_2(tz\text{-}tol)_4]$ (1) and $[Cu_2(tz\text{-}naf)_4]$ (2). The molecular drawings of the $[Cu_2(tz\text{-}tol)_4]$ (**1**) and $[Cu_2(tz\text{-}naf)_4]$ (**2**) complexes with the atomic numbering scheme are shown in Figures 1 and 2, respectively. Selected structural parameters for the two compounds are listed in Table 2. The structures of **1** and **2** consist of dimer units. In both complexes each copper atom of the dinuclear entity is four-coordinated with a slightly distorted square planar environment. The copper(II) ions are linked to two thiazole N atoms of two sulfonamidate ligands (tz-tol$^-$ in **1** and tz-naf$^-$ in **2**) and two sulfonamido N atoms from other two sulfonamidate anions. In the coordination polyhedra the $N_{thiazole}$ atoms are in trans position. In the dinuclear species the metal ions are bridged by four triatomic NCN groups. For the two compounds the metal−ligand distances Cu−$N_{thiazole}$ (ca. 1.94 Å in **1** and ca. 1.96 Å in **2**) are shorter than the Cu−$N_{sulfonamido}$ ones (ca. 2.07 Å in **1** and ca. 2.03 Å in **2**). These bond lengths compare well with those for previously reported N-substituted sulfonamide copper complexes.[5,6,8,12] Bond angles of the CuN_4 chromophores are close to 90° and range from 87.98(15) to 92.30(15)° in **1** and from 86.98(15) to 90.89(15)° in **2**. In compound **1** the Cu(II) ion is displaced 0.2182(21) Å above the mean plane formed by N(11), N(21a), N(12a), and N(22) atoms. In complex **2** the Cu1 atom is placed 0.1847(20) Å above the plane formed by N(12), N(21), N(32), and N(41)

(30) Casanova, J.; Alzuet, G.; Ferrer, S.; Borrás, J.; García-Granda, S.; Perez-Carreño, E. J. *Inorg. Biochem.* **1993**, *51*, 689.
(31) Pedregosa, J. C.; Casanova, J.; Alzuet, G.; Borrás, J.; García-Granda, S.; Gutiérrez Rodríguez. A. *Inorg. Chim. Acta* **1995**, *232*, 117.

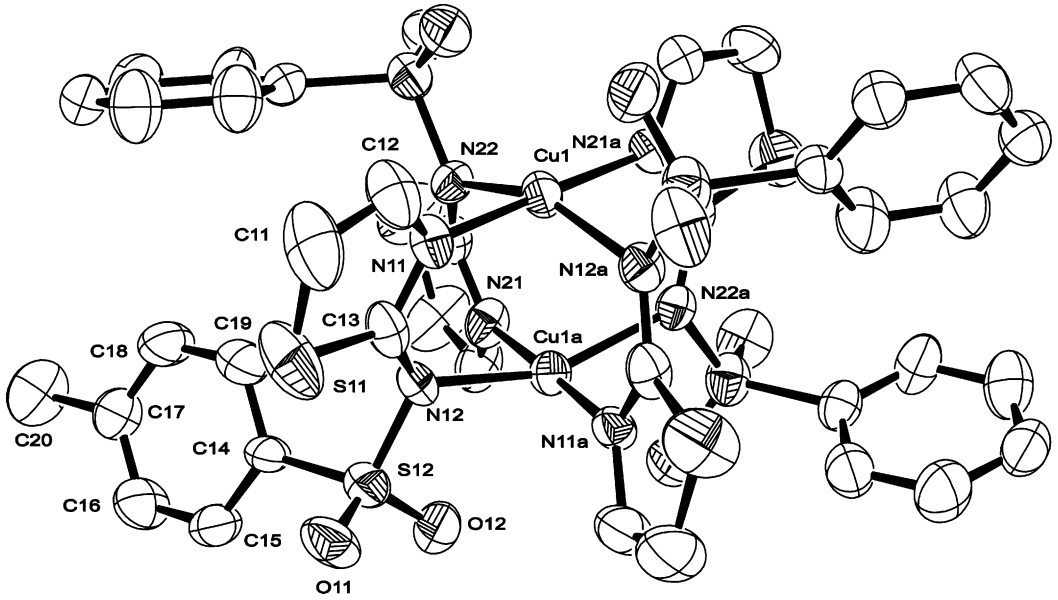

Figure 1. Molecular structure of $[Cu_2(tz\text{-}tol)_4]$.

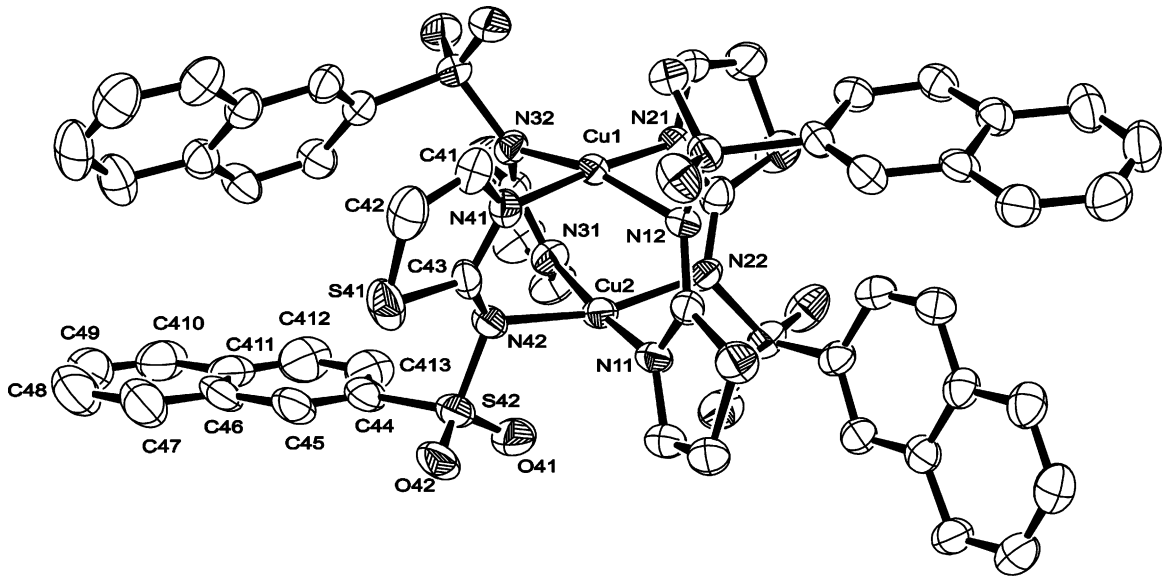

Figure 2. Molecular structure of $[Cu_2(tz\text{-}naf)_4]$.

atoms, which are arranged in a regular square plane, and the Cu2 atom is located 0.1998(21) Å above the mean plane formed by N(11), N(22), N(31), and N(42) atoms. The Cu···Cu distances, 2.7224(13) Å in **1** and 2.6257(10) Å in **2**, are in the range found for dinuclear copper(II) compounds with four NCN bridges.[9−11] It is noteworthy that the metal−metal distance in **2** is very short, comparable with the Cu···Cu distance in the structurally related $[Cu_2(sulfathiazolato)_4]$ complex.[9] In $[Cu_2(tz\text{-}tol)_4]$ (**1**) and $[Cu_2(tz\text{-}naf)_4]$ (**2**) the two CuN_4 planes of each compound show a parallel arrangement. For **1** the dihedral angle between the two CuN_4 planes is 0° since this complex has a binary axis perpendicular to the center of Cu···Cu distance, and for **2** the dihedral angle between the two CuN_4 mean planes is 1.49(21)°.

The square planar geometry of the copper(II) ions in both compounds presents tetrahedral distortion. Tetrahedrality for any tetracoordinate copper complex can be characterized by the angle subtended by two planes, each encompassing the copper and two donor atoms.[32] For strictly square planar complexes with D_{4h} symmetry, the value is 0°, while, for regular tetrahedral complexes, the angle is 90°. The tetrahedrality value of 24.29(22)° for the $[Cu_2(tz\text{-}tol)_4]$ compound indicates a higher distortion from the square planar geometry than the tetrahedrality values of 16.28(24)° [Cu1] and 17.40(26)° [Cu2] for the $[Cu_2(tz\text{-}naf)_4]$ complex.

The tz-tol$^-$ anions in **1** and the tz-naf$^-$ anions in **2** act as bridging bidentate ligands, linking one Cu(II) by the thiazole N atom and the other Cu(II) through the sulfonamidate N atom. In general, the internal geometry of the tz-tol$^-$ and tz-naf$^-$ compares well with that of the corresponding protonated ligands (Htz-tol, Htz-naf); only a slight lengthening of the $C_{thiazole}-N_{sulfonamido}$ bond distances and a slight

(32) Battaglia, L. P.; Bonamartini-Corradi, A.; Marcotrigiano, G.; Menabue, L.; Pellacani, G. C. *Inorg. Chem.* **1979**, *18*, 148.

Table 2. Selected Bond Distances (Å) and Angles (deg) for $[Cu(tz\text{-}tol)_2]_2$ (**1**) and $[Cu(tz\text{-}naf)_2]_2$ (**2**)[a]

$[Cu(tz\text{-}tol)_2]_2$		$[Cu(tz\text{-}naf)_2]_2$	
Cu(1)−N(21)$^{\#1}$	1.942(4)	Cu(1)−N(21)	1.965(4)
Cu(1)−N(11)	1.947(4)	Cu(1)−N(41)	1.969(4)
Cu(1)−N(12)$^{\#1}$	2.067(4)	Cu(1)−N(32)	2.024(4)
Cu(1)−N(22)	2.088(4)	Cu(1)−N(12)	2.047(4)
Cu(1)−Cu(1)$^{\#1}$	2.7224(13)	Cu(1)−Cu(2)	2.6257(10)
		Cu(2)−N(11)	1.963(4)
		Cu(2)−N(31)	1.988(4)
		Cu(2)−N(22)	2.018(4)
		Cu(2)−N(42)	2.055(4)
N(21)$^{\#1}$−Cu(1)−N(11)	178.04(17)	N(21)−Cu(1)−N(41)	173.89(17)
N(21)$^{\#1}$−Cu(1)−N(12)$^{\#1}$	90.11(16)	N(21)−Cu(1)−N(32)	86.98(15)
N(11)−Cu(1)−N(12)$^{\#1}$	87.98(15)	N(41)−Cu(1)−N(32)	90.89(15)
N(21)$^{\#1}$−Cu(1)−N(22)	89.63(15)	N(21)−Cu(1)−N(12)	90.19(15)
N(11)−Cu(1)−N(22)	92.30(15)	N(41)−Cu(1)−N(12)	90.38(15)
N(12)$^{\#1}$−Cu(1)−N(22)	155.71(15)	N(32)−Cu(1)−N(12)	164.78(15)
N(21)$^{\#1}$−Cu(1)−Cu(1)$^{\#1}$	91.08(14)	N(11)−Cu(2)−N(31)	173.13(16)
N(11)−Cu(1)−Cu(1)$^{\#1}$	88.99(13)	N(11)−Cu(2)−N(22)	90.47(16)
N(12)$^{\#1}$−Cu(1)−Cu(1)$^{\#1}$	78.50(11)	N(31)−Cu(2)−N(22)	87.75(16)
		N(11)−Cu(2)−N(42)	89.14(16)
		N(31)−Cu(2)−N(42)	90.76(16)
		N(22)−Cu(2)−N(42)	164.07(15)

[a] Symmetry transformation used to generate equivalent atoms: (#1) $-x$, y, $-z + 1/2$.

shortening of the $C_{thiazole}-N_{thiazol}$ bond lengths due to deprotonation and coordination can be appreciated.

Spectroscopic and Electrochemical Properties. The IR spectra of the Cu(II) complexes show similar pattern of bands. Compared with the IR spectra of the free ligands, the most remarkable difference occurs in the band corresponding to the stretching vibration of the thiazole ring, which is shifted from 1540 cm^{-1} in the free ligands to ca. 1470 cm^{-1} in the complexes. The $\nu(SO_2)_{as}$ and $\nu(SO_2)_s$ bands do not show significant shifts with respect to those of the ligands. The characteristic band corresponding to the ν(S−N) appears to be shifted by ca. 14 cm^{-1} (compound **1**) and 26 cm^{-1} (compound **2**) to higher frequencies.

The diffuse reflectance spectra of the two complexes show a very broad and intense band around 500 nm, characteristic of a CuN_4 chromophore with the copper ion in a square planar environment.[33] The electronic spectra of the complexes in CH_3CN and in acetone display a maximum at ca. 490 nm for **1** and at ca. 500 nm for **2**. As no significant changes occur in the position of d−d bands upon dissolution of the complexes, this indicates the absence of significant modifications in the coordination sphere of the metal ions.

The electrochemical behavior of both complexes was investigated by cyclic voltammetry in acetonitrile solution. When we scan toward the negative potentials, the cyclic voltammogram curve of complex **1** is characterized by one irreversible electrochemical signal at $E_{pc} = -394$ mV that corresponds to the reduction $Cu^{II}{}_2/Cu^{I}{}_2$. Accordingly, in the reverse scan, a sharp anodic peak is found at −24 mV which can be attributed to oxidation of two copper(I) ions. For complex **2**, the cathodic part of the cyclic voltammogram reveals two successive irreversible electrochemical signals. The first weak signal at −198 mV is assigned to the reduction $Cu^{II}{}_2/Cu^{II}Cu^{I}$ and the second at −377 mV to the reduction process $Cu^{II}Cu^{I}/Cu^{I}{}_2$. In the reverse scan, an anodic peak at −41 mV due to the two copper(I) oxidation is observed. The irreversibility of the electrochemical processes was thought to be caused by changes in the coordination sphere around the metal center upon reduction.

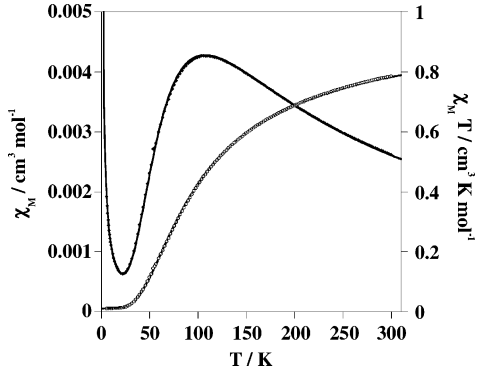

Figure 3. Temperature dependence of χ_M (●) and $\chi_M T$ (○) for $[Cu_2(tz\text{-}tol)_4]$. The solid lines represent the fitted function.

Magnetic Properties. Magnetic susceptibility measurements of **1** and **2** were performed on crystals in the temperature range 2−350 K. The temperature dependence of the magnetic susceptibility/Cu of the $[Cu_2(tz\text{-}tol)_4]$ compound is shown in Figure 3. The $[Cu_2(tz\text{-}naf)_4]$ complex exhibits the same magnetic behavior (data not shown). The dominant features of the plots are a maximum around 100 K and a rapid decrease to zero at lower temperatures. The solid curve in Figure 3 is the best fit of the data to the Bleaney−Bowers equation[34] for the exchange-coupled copper(II) dimers,

$$\chi_M = (Ng^2\beta^2/kT)[3 + \exp(-2J/kT)]^{-1}(1 - \rho) + \rho Ng^2\beta^2/4kT + \chi_{TIP} \quad (1)$$

which results from a consideration of the eigenvalues of $H = -2JS_1S_2$ and where the symbols have the usual meanings. An excellent fit was obtained when $-2J = 121.3$ cm^{-1}, $g = 2.19$, $\chi_{TIP} = 120 \times 10^{-6}$, $\rho = 0.022$, and $R = 3.5 \times 10^{-5}$ for compound **1** and $-2J = 104.3$ cm^{-1}, $g = 2.13$, $\chi_{TIP} = 120 \times 10^{-6}$, $\rho = 0.006$, and $R = 1.2 \times 10^{-4}$ for compound **2**.

The antiferromagnetic coupling constant of both compounds is larger than that of the related $[Cu_2(sulfathiazolato)_4]$ complex ($-2J = 61.5$ cm^{-1}). No direct correlation is found between the magnitude of the coupling constant and the Cu···Cu distance (**1**, 2.7224 Å; **2**, 2.6257 Å; $[Cu_2(sulfathiazolato)_4]$, 2.671 Å). Moreover, it should be noted that the antiferromagnetic exchange coupling constants of **1** and **2** are smaller than that of copper(II) dimers with adenine and its derivatives.[10,11] In this sense, the magnetic behavior of $[Cu_2(tz\text{-}tol)_4]$ and $[Cu_2(tz\text{-}naf)_4]$ is in good agreement with the theoretical results previously reported by us[12] for dinuclear copper(II) compounds with NCN bridges belonging to ligands with two condensed ring (adenine) or with one single ring (sulfathiazole or sulfamethazine).

(33) Ravichandran, V.; Chacko, K. K.; Aoki, A.; Yamazaki, H.; Ruiz-Sánchez, J.; Suarez-Varela, J.; López-Gonzalez, J. D.; Salas-Peregrín, J. M.; Colacio-Rodriguez, E. *Inorg. Chim. Acta* **1990**, *173*, 107.

(34) Bleaney, B.; Bowers, K. D. *Proc. R. Soc. London, Ser. A* **1952**, *214*, 451.

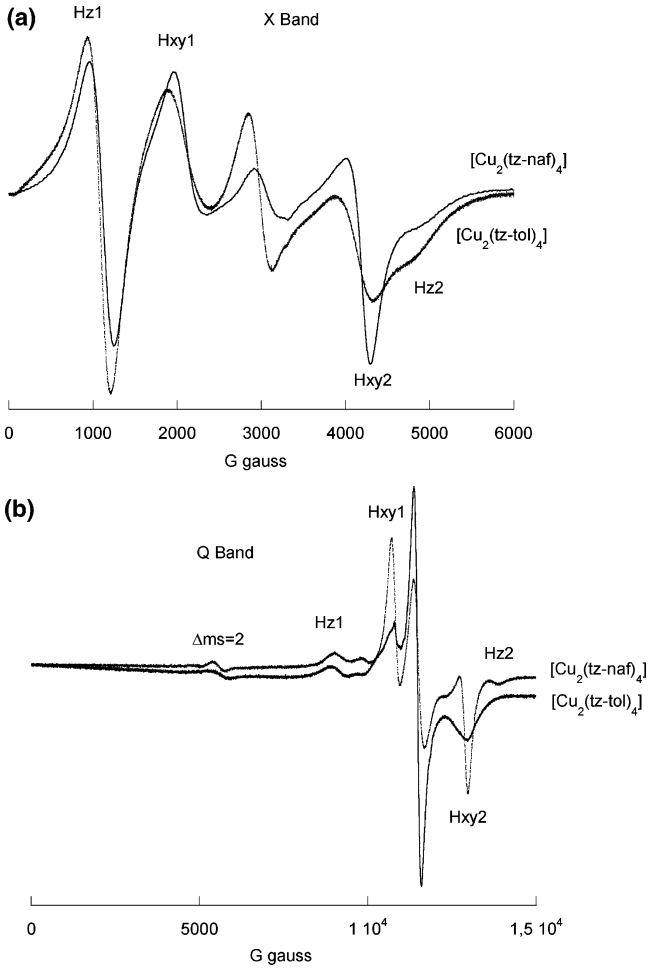

Figure 4. (a) X-band powder EPR spectra of $[Cu_2(tz\text{-}tol)_4]$ and $[Cu_2(tz\text{-}naf)_4]$ at 290 K. (b) Q-band powder EPR spectra of $[Cu_2(tz\text{-}tol)_4]$ and $[Cu_2(tz\text{-}naf)_4]$ at 290 K.

EPR. The solid-state EPR spectra of the complexes obtained at room temperature at the X- and Q-band (Figure 4) show signals typical for coupled binuclear complexes,[35,36] together with the characteristic signal for a monomeric species at ~3300 G (Figure 4a) and at ~11 300 G (Figure 4b). The formation of a binuclear complex is connected with antiferromagnetic coupling of two Cu(II) ions, leading to a singlet ground state and an excited spin triplet state. The energy difference, $2J$, between these states depends on the strength of the interaction. If the triplet state is thermally accessible ($2J \approx kT \approx 200-400$ cm^{-1}) paramagnetism is observed and the EPR spectra could be satisfactorily described using the interactive spin Hamiltonian for isolated Cu(II) dimers ($S = 1$):

$$H = g\beta BS + DS_{z^2} + E(S_{x^2} - S_{y^2}) - 2D/3 \qquad (2)$$

Here, D and E are the zero field splitting parameters, β is the Bohr magneton, and x, y, and z are the principal axes of the coordinating system, fixed with respect to the Cu···Cu bond. Wasson et al.[35] showed that, in the case of powder samples, two transitions allowed by the selection rule ($\Delta m_s = \pm 1$) will result in each principal direction and six resonance fields can be determined. Furthermore, a transition with ($\Delta m_s = \pm 2$) is also obtained. The six resonance fields are H_{x^1}, H_{x^2}, H_{y^1}, H_{y^2}, H_{z^1}, and H_{z^2}, whose equations are proposed by Wasserman et al.[36] for a rhombic symmetry ($E \neq 0$). For an axial symmetry ($E = 0$), when $D < h\nu$, as is usual in the case of copper dimers, four $\Delta m_s = \pm 1$ transitions along with a half-field ($\Delta m_s = \pm 2$) transition are allowed. These four resonance fields are H_{z^1}, H_{xy^1}, H_{xy^2}, and H_{z^2}, which are given by the following equations:

$$H_{z^1} = (g_e/g_z)(H_0 - D') \qquad (3)$$

$$H_{xy^1} = (g_e/g_z)^2 H_0(H_0 - D') \qquad (4)$$

$$H_{xy^2} = (g_e/g_z)^2 H_0(H_0 + D') \qquad (5)$$

$$H_{z^2} = (g_e/g_z)(H_0 + D') \qquad (6)$$

The X-band EPR spectrum of $[Cu_2(tz\text{-}tol)_4]$ (**1**) at room temperature (Figure 4a) shows transitions at 932, 1874, 4324, and at 4822 G, the last one occurring as a shoulder. At the Q-band, the spectrum of **1** displays peaks at 8980, 10 800, and 12 960 G (Figure 4b). The X-band EPR spectrum of $[Cu_2(tz\text{-}naf)_4]$ (**2**) at room temperature (Figure 4a) exhibits peaks at 996, 2009, and 4261 G and a shoulder at 4800 G. At the Q-band the spectrum of **2** shows transitions at 9000, 10 700, 12 970, and 13 850 G (Figure 4b). These signals, assigned to the resonance fields H_{z^1}, H_{xy^1}, H_{xy^2}, and H_{z^2}, respectively, are indicative of copper centers with an axial symmetry, in agreement with the crystal structures. In addition, the formally forbidden transition ($\Delta m_s = \pm 2$), the so-called half-field spin transition, is observed at the Q-band at 5607 G for $[Cu_2(tz\text{-}tol)_4]$ and at 5580 G for $[Cu_2(tz\text{-}naf)_4]$.

From the observed transitions Hz^1, H_{xy^1}, H_{xy^2}, and H_{z^2} and the half-field spin transitions[37] the calculated parameters are the following: $D = 0.230$ cm^{-1}, $g_{\|} = 2.35$, $g_{\perp} = 2.08$ (compound **1**); $D = 0.229$ cm^{-1}, $g_{\|} = 2.25$, $g_{\perp} = 2.07$ (compound **2**). The D value is of the same order of magnitude as that of the structurally related $[Cu_2(stz)_4]$ complex.[9]

The X-band EPR spectra of both complexes were recorded at different temperatures. The spectra of the $[Cu_2(tz\text{-}naf)_4]$ (**2**) complex at 290, 70, and 20 K are shown in Figure 5. The spectra of $[Cu_2(tz\text{-}tol)_4]$ (**1**) in the same conditions are similar (data not shown). At 10 K the EPR of the two complexes are silent. For both compounds, the peaks in the EPR spectrum at room temperature are clearly much broader than those of the spectra at 70 K, a temperature close to that of the maximum in the magnetic measurements. At high temperatures, the triplet states are relatively more populated and the dimer signals are broader due to short electron-spin relaxation times (T_{1e}) and to intermolecular interactions. When the temperature decreased to 20 K, the spectrum became narrower and seven hyperfine features with a relative intensity of 1:2:3:4:3:2:1, due to two interacting Cu(II) ions

(35) Wasson, J. R.; Chin-I, S.; Trapp, C. *Inorg. Chem.* **1968**, *7*, 469.
(36) Wasserman, E.; Snyder, L. C.; Yager, W. A. *J. Chem. Phys.* **1964**, *41*, 1763.
(37) Eaton, S. A.; More, K. M.; Sawant, B. M.; Eaton, G. R. *J. Am. Chem. Soc.* **1983**, *105*, 6550.

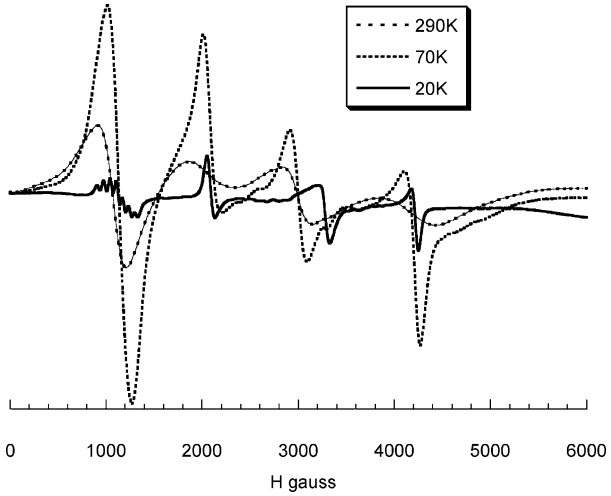

Figure 5. X-band powder EPR spectra of $[Cu_2(tz\text{-}naf)_4]$ at 290, 70, and 20 K.

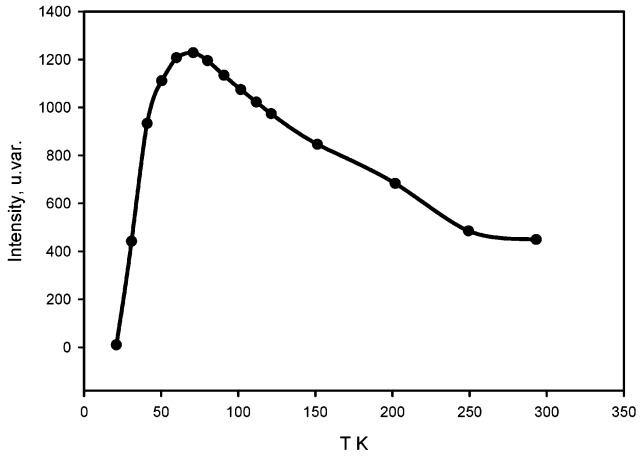

Figure 6. Temperature dependence of the intensity of the $H_{z'}$ EPR signal for the $[Cu_2(tz\text{-}tol)_4]$ complex.

$(2nI + 1; n = 2$ and $I = 3/2)$ are observed in the low-field components. The separation between these lines is approximately 67 G and is just a half of the hyperfine splitting evident on the line corresponding to the free copper ion. This is just what is to be expected from a line, the origin of which is due to an exchange interaction.[38]

For evaluation of the exchange interaction parameter, $2J$, the variation of the intensity of the EPR signals with the temperature was studied for the two complexes. Figure 6 shows the integral intensity of the $H_{z'}$ peak at the temperatures from 293 to 20 K for compound **1**. The relative intensity of the absorption is given by[35]

$$R \propto 1/T(e^{-2J/kT})/(1 + 3e^{-2J/kT}) \qquad (7)$$

From the plots, the values of $-2J = 123.76$ cm^{-1} for $[Cu_2(tz\text{-}tol)_4]$ and $-2J = 94.87$ cm^{-1} for $[Cu_2(tz\text{-}naf)_4]$ were obtained; these values are very close to those obtained from magnetic measurements.

In frozen acetonitrile solution the X-band EPR spectrum of complex **1** shows a very weak signal whose pattern is

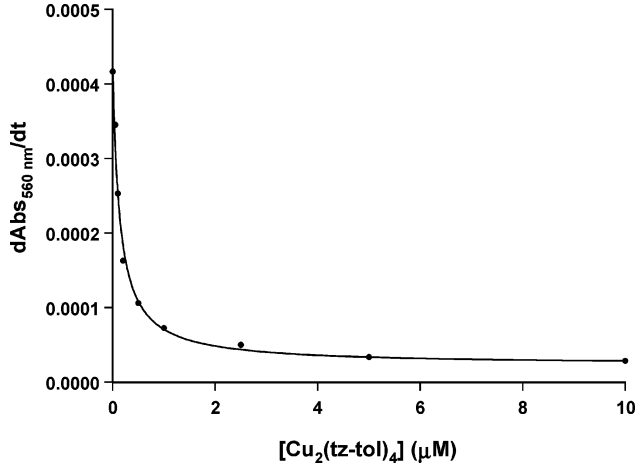

Figure 7. SOD activity study of the complex $[Cu_2(tz\text{-}tol)_4]$: Dependence absorbance changes with time at 560 nm as a function of $[Cu_2(tz\text{-}tol)_4]$ concentration.

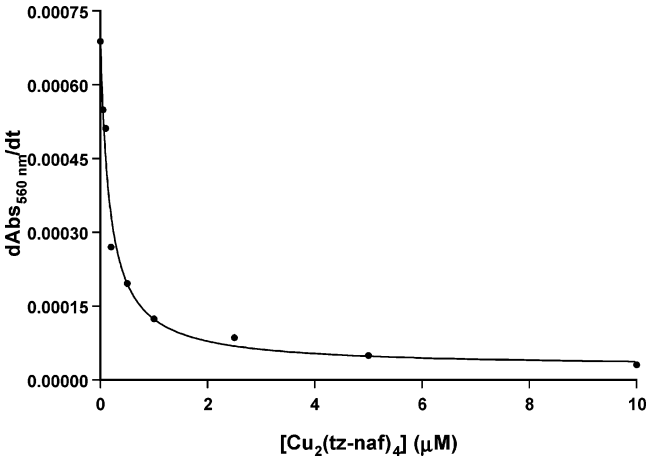

Figure 8. SOD activity study of the complex $[Cu_2(tz\text{-}naf)_4]$: Dependence absorbance changes with time at 560 nm as a function of $[Cu_2(tz\text{-}naf)_4]$ concentration.

characteristic of mononuclear species with a square planar CuN_4 chromophore. In the parallel region a hyperfine structure with $A_{\|}$ value of 151×10^{-4} cm^{-1} is observed. Also, in the perpendicular region, nine signals attributed to the superhyperfine coupling of the four nitrogen with $A^N_{\perp} = 14 \times 10^{-4}$ cm^{-1} are clearly resolved.[39] In frozen acetone solution the X-band EPR spectrum of complex **1** exhibits weak signals at 1966 G and at 4281 G. These signals are almost coincident with the corresponding ones in the EPR spectrum of the polycrystalline sample which indicates that the dimeric species remains in solution.

Superoxide Dismutase Activity. Kinetic studies of the SOD reaction by $[Cu_2(tz\text{-}tol)_4]$ and $[Cu_2(tz\text{-}naf)_4]$ complexes were carried out using the xanthine/xanthine oxidase/NBT assay system. NBT acts as superoxide detecting agent through its reduction to MF^+. Figures 7 and 8 show that the rate of the absorbance development at 560 nm with time is reduced in the presence of $[Cu_2(tz\text{-}tol)_4]$ and $[Cu_2(tz\text{-}naf)_4]$, respectively, in a concentration-dependent behavior. This indicates that in the presence of both dinuclear complexes the steady-state concentration of superoxide is reduced; thus,

(38) Slichter, C. P. *Phys. Rev.* **1955**, *99*, 479.

(39) Wieserma, A. K.; Windle, J. J. *J. Phys. Chem.* **1964**, *68*, 2316.

$[Cu_2(tz\text{-}tol)_4]$ and $[Cu_2(tz\text{-}naf)_4]$ exhibit significant catalytic activity toward the dismutation of superoxide.

In the presence of the copper complex the mechanism of the reduction of NBT to MF^+ comprises several reactions. The system xanthine/xanthine oxidase produces superoxide ion that undergoes self-degradation via a bimolecular reaction but also reacts with NBT to produce MF^+. At the same time the copper complex interacts with $O_2^{\bullet-}$ catalyzing its dismutation to molecular oxygen and hydrogen peroxide; this reaction reduces the superoxide concentration in solution and, thus, the MF^+ production rates (i.e. slowing down absorbance variation). The development of hydrogen peroxide in the presence of the copper complexes could give rise to the formation of reactive species which may be responsible for a new path for the formation of MF^+. In fact, Figures 7 and 8 show that even in the presence of a large concentration of the copper complexes, the MF^+ formation rate does not fall completely to zero but reaches a small, constant value. This residual absorbance variation can be accounted for considering that in the presence of high concentration of copper complex all superoxide is rapidly dismutated in solution (to a very little steady-state concentration) to O_2 and H_2O_2. The peroxide generated, through the formation of copper active species, is responsible for the residual color development observed.

The complete kinetic study of the SOD activity of $[Cu_2(tz\text{-}tol)_4]$ and $[Cu_2(tz\text{-}naf)_4]$ is complicated by the large number of processes involved. But our experimental conditions allow some simplifications. The xanthine oxidase and NBT concentrations have been optimized to give a linear absorbance increase during the assay; i.e., the superoxide concentration in solution remains stationary during the assay. If we assume that the binding of superoxide by the copper complexes is fast, the fraction of free and copper-bound superoxide is ruled by the copper complex concentration and by the affinity constant (K) for the copper complex/$O_2^{\bullet-}$ adduct formation. The free superoxide reacts with NBT through the classical mechanism while the copper complex/$O_2^{\bullet-}$ adduct produces MF^+ in a less efficient reaction via hydrogen peroxide generation:

$$\text{xanthine} + \text{xanthine oxidase} \rightarrow O_2^{\bullet-} \tag{8}$$

$$O_2^{\bullet-} + \text{NBT} \rightarrow MF^+ \tag{9}$$

$$O_2^{\bullet-} + \text{Cu} \rightleftarrows CuO_2 \tag{10}$$

$$CuO_2 \rightarrow\rightarrow H_2O_2 \rightarrow\rightarrow MF^+ \tag{11}$$

Here Cu is either $[Cu_2(tz\text{-}tol)_4]$ or $[Cu_2(tz\text{-}naf)_4]$ and CuO_2 represents the adduct between superoxide and $[Cu_2(tz\text{-}tol)_4]$ or $[Cu_2(tz\text{-}naf)_4]$. The kinetic parameters for the SOD activity of the complexes were obtained by fitting the absorbance changes with time with eq 12 (see Appendix for its derivation):

$$\frac{d\text{Abs}}{dt} = \text{constant} \cdot \frac{1 + fK[\text{Cu}]_{\text{TOT}}}{1 + K[\text{Cu}]_{\text{TOT}}} \tag{12}$$

Table 3. SOD Activity of Copper Complexes

compd	IC_{50} (μM)	ref
$[Cu_2(tz\text{-}tol)_4]$	0.13 ± 0.02	present work
$[Cu_2(tz\text{-}naf)_4]$	0.17 ± 0.04	present work
$[Cu(im)Cu(pip)_2]^{3+}$	0.5	40, 41
$[Cu_2(bdpi)(CH_3CN)_2]^{3+}$	0.32	42
$[Cu_2(Me_4bdpi)(H_2O)_2]^{3+}$	1.1	42
$[CuZn(bdpi)(CH_3CN)_2]^{3+}$	0.24	42
native CuZnSOD	0.0012−0.0081	43−46

Here the constant depends on the xanthine, xanthine oxidase, and NBT concentrations and on the MF^+ extinction coefficient; K is the affinity constant of superoxide for the copper complexes, $[Cu]_{TOT}$ is the total concentration of copper complex (free complex plus superoxide bound complex), and f indicates the relative efficiency of reaction 11, with respect to reaction 9, in the formation of MF^+. Equation 12 fits well the experimental data. The parameters obtained are the following: for $[Cu_2(tz\text{-}tol)_4]$, $K = 7.5 \pm 1.0\ \mu M^{-1}$, $f = 0.05 \pm 0.02$; for $[Cu_2(tz\text{-}naf)_4]$, $K = 6.0 \pm 1.0\ \mu M^{-1}$, $f = 0.04 \pm 0.03$.

The most important result is that both complexes efficiently catalyze superoxide dismutation below the micromolar concentration range. Moreover, despite the relatively large standard deviation, the f values show that the mechanism via hydrogen peroxide is 20 times less efficient in promoting MF^+ formation with respect to that of reaction 10. To better emphasize this result, it is convenient to express the SOD activity of the complexes as IC_{50} values (the concentration of the complex required to attain 50% inhibition of the reduction). The IC_{50} value can be obtained from the reciprocal of the K values. Table 3 compares the data obtained for $[Cu_2(tz\text{-}tol)_4]$ and for $[Cu_2(tz\text{-}naf)_4]$ with the IC_{50} values of the best copper SOD mimics so far reported[40−42] and the value for native SOD[43−46] (note that the smaller the IC_{50} value, the higher the SOD activity). The IC_{50} value exhibited by the present complexes is smaller than those reported for any copper SOD mimics so far and approaches the activity of the enzyme. The remarkable SOD activity observed with $[Cu_2(tz\text{-}tol)_4]$ and $[Cu_2(tz\text{-}naf)_4]$ is probably related to the presence of two coupled copper(II) ions in close proximity. One Cu(II) may resemble the role of Zn(II) in the native SOD which, through the imidazolate bridge, controls the electron density at the redox active Cu(II).

Appendix

The effect of the copper complexes on the MF^+ formation in the xanthine oxidase/NBT assay can be accounted for considering the following mechanism:

(40) Bienvenue, E.; Choua, S.; Lobo-Racio, M.-A.; Marzin, C.; Pacheco, P.; Seta, P.; Tarrago, G. *J. Inorg. Biochem.* **1995**, *57*, 157.
(41) Weser, U.; Schubotz, L. M.; Lengfelder, E. *J. Mol. Catal.* **1981**, *13*, 249.
(42) Ohtsu, H.; Shimazaki, Y.; Odani, A.; Yamauchi, O.; Mori, W.; Itoh, S.; Fukuzumi, S. *J. Am. Chem. Soc.* **2000**, *122*, 5733.
(43) McCord, J. M.; Fridovich, I. *J. Biol. Chem.* **1969**, *244*, 6049.
(44) Butler, J.; Koppenol, W. H.; Margoliasch, E. *J. Biol. Chem.* **1982**, *257*, 10747.
(45) Muller, J.; Schubl, D.; Maischle-Mosser, C.; Strahle, J.; Wesser, U. *J. Inorg. Biochem.* **1999**, *75*, 63.
(46) Kovala-Demertzi, D.; Galani, A.; Demertzis, M. A.; Skoulika, S.; Kotoglou, C. *J. Inorg. Biochem.* **2004**, *98*, 358.

$$\text{xanthine} + \text{xanthine oxidase} \rightarrow O_2^{\bullet -} \quad \text{(S1)}$$

$$O_2^{\bullet -} + Cu \rightleftarrows CuO_2 \quad \text{(S2)}$$

$$O_2^{\bullet -} + NBT \rightarrow MF^+ \quad \text{(S3)}$$

$$CuO_2 \rightarrow\rightarrow H_2O_2 \rightarrow\rightarrow MF^+ \quad \text{(S4)}$$

Here Cu is the copper complex and CuO_2 represents its adduct with superoxide. Reaction S1 provides, under the conditions employed, a constant flux of superoxide. The MF^+ formation occurs through reactions S3 and S4. The rate of reaction S3 depends on the NBT concentration (which remains approximately constant during the assay) and on the fraction of free superoxide present in solution and is given by

$$\text{rate}_{S3} = R_{S3}[O_2^{\bullet -}] \quad \text{(S5)}$$

where R_{S3} depends on [NBT]. The rate of reaction S4 depends on the fraction of superoxide bound to the copper complex. If we indicate with f the relative efficiency of reaction S4 with respect to reaction S3, the rate of the former process is

$$\text{rate}_{S4} = fR_{S3}[CuO_2] \quad \text{(S6)}$$

In the proposed scheme, reaction S2 is considered a fast equilibrium step (faster than reactions S3 and S4) so the concentrations of $O_2^{\bullet -}$, CuO_2, and Cu are ruled by the affinity constant K and the mass balance on superoxide and the copper complex. Since during the assay the steady-state concentration of superoxide is maintained very low, the fraction of the complex bound to the anion can be considered much lower than the total copper complex, $[Cu]_{TOT}$ ($[Cu]_{TOT} = [Cu] + [CuO_2] \approx [Cu]_{TOT}$). Therefore, we can write

$$[O_2^{\bullet -}] = \frac{[O_2^{\bullet -}]_{TOT}}{1 + K[Cu]_{TOT}} \quad \text{(S7)}$$

$$[CuO_2] = \frac{[O_2^{\bullet -}]_{TOT} K[Cu]_{TOT}}{1 + K[Cu]_{TOT}} \quad \text{(S8)}$$

where $[O_2^{\bullet -}]_{TOT}$ is the total superoxide concentration (free plus copper bound superoxide) as supplied by the xanthine oxidase/xanthine system.

The global formation rate of MF^+ is given by the sum of rate_{S3} and rate_{S4}; thus, combining equations from S5 to S8, we obtain

$$\text{rate} = R_{S3}[O_2^{\bullet -}]_{TOT} \frac{1 + fK[Cu]_{TOT}}{1 + K[Cu]_{TOT}} \quad \text{(S9)}$$

The spectral variation due to the formation of MF^+ with time can be obtained from eq S9 through the Lambert−Beer equation. If the steady-state concentration of superoxide is maintained constant during the experiment, $[O_2^{\bullet -}]_{TOT}$ can be combined with R_{S3}, the extinction coefficient of the product, and the cuvette path length to give a single constant:

$$\frac{\text{dAbs}}{dt} \text{constant} \cdot \frac{1 + fK[Cu]_{TOT}}{1 + K[Cu]_{TOT}} \quad \text{(S10)}$$

Acknowledgment. J.B., G.A., and S.F. acknowledge financial support from the Spanish CICYT (Grant BQU2001-3173-C02-01), and R.C.-M. acknowledges support by the "MEBIOS" Marie Curie training site. The authors also thank COSTD21 for support, S. García-Granda and H. Rodriguez-Prieto (University of Oviedo) for crystallographic determination of the Htz-tol ligand, and J. A. Real (University of Valencia) for magnetic measurements.

Supporting Information Available: Details of the X-ray structure determinations of Htz-tol, Htz-naf, and the complexes as CIF files. The material is available free of charge via the Internet at http://pubs.acs.org.

IC049718W